Finite Element Analysis of Three-Dimensional Transient Heat Transfer in GMA Welding

The data generated in this study can be used to determine the heating and cooling rate, weld pool shape and HAZ

BY P. TEKRIWAL AND J. MAZUMDER

ABSTRACT. The thermal history of a weld joint produced by the gas metal arc (GMA) welding process is analyzed by using a three-dimensional finite element model. The problem consists of one in which the finite element mesh is growing continuously in time in order to accommodate metal transfer in GMA welding. The procedure of how to incorporate the growth of the mesh in the analysis has been described.

The finite element program ABAQUS, along with a few user subroutines, was employed to obtain the numerical results. Temperature-dependent thermal properties, effect of latent heat, and the convective and radiative boundary conditions are included in the model. Numerically predicted sizes of the heat-affected zone and the melt-pool zone are compared with the experimentally observed values.

Introduction

Welding technology has been by and large empirical to date. Experiments and experience have contributed to the present state-of-the-art in welding (Ref. 1). But with the advent of the computer age, efforts are being made to make available to practicing engineers the science behind welding. The effort to quantify heat flow and residual stresses in welding goes back to the 1930's when Rosenthal (Refs. 2, 3) and Boulton and Martin (Ref. 4) developed analytical models for the theory of welding. These analytical models are of little practical use to design engineers as they are too idealized to be used in practice. Nevertheless, these methods have provided a foundation for the numerical methods that can take into account the nonlinearities involved in the process and provide a practical solution. The finite element method has developed into a powerful tool to solve problems governed by differential equations (Ref. 5), including transient heat conduction analysis of complex shapes (Refs. 6, 7). While the technique has been used fairly well to simulate and model the gas tungsten arc welding (GTAW) process by Friedman (Refs. 8–10), Krutz, *et al.* (Ref. 11), Tekriwal, *et al.* (Ref. 13), and Mahin, *et al.* (Ref. 14), not many attempts have been made to model a gas metal arc welding process. Hibbitt and Marcal (Ref. 12) analyzed an axisymmetrical example with addition of molten filler material. However, the material properties were updated only periodically in their model. The work presented here, to the best of the authors' knowledge, is the first three-dimensional transient, moving heat source heat transfer analysis for the GMA welding process. Details of the finite element formulation are reported elsewhere (Ref. 13). The material properties are updated on a more continuous basis after each iteration in the solution. The results of the analysis are evaluated in terms of the comparison of the size of the heat-affected zone (HAZ) and the melt-pool zone (MPZ) with the experimental observation — Table 1. Numerical data used for the welding parameters were supplied by the U.S. Army Construction Engineering Research Laboratory, Champaign, Ill., and the experiment was conducted on samples at their facility.

KEY WORDS

GMAW Heat Transfer
Three-Dimensional
Transient Heat
Finite Element Model
ABAQUS
Thermal Properties
Latent Heat Effect
Boundary Conditions
Convective-Radiative

GMA Welding Process

Figure 1 depicts the GMAW process, in which a constant supply of the consumable electrode is maintained through the center of the welding nozzle. When the electrode comes close to the workpiece, an arc is produced, which causes the electrode tip to melt and join the V-groove between the two plates. A constant supply of the shielding gas (98% argon and 2% oxygen) is also maintained through the annulus around the feedwire inside the nozzle, protecting the weld from atmospheric contamination.

With regard to modeling the process, the following may be noted.

1) A part of the heat supplied by the

Table 1—Comparison of Numerical and Experimental Results

Quantity	Numerical Value	Experimental Value	Difference
HAZ	32.0 mm	31.7 mm	0.9%
MPZ	15.4 mm	16.8 mm	8.3%
Peak temperature at a point	1200 K	1115 K	7.6%

P. TEKRIWAL and J. MAZUMDER are with the Department of Mechanical and Industrial Engineering, University of Illinois at Urbana-Champaign, Urbana, Ill.

arc is consumed to melt the welding wire continuously.

2) A part of the heat is lost to the surroundings before it is received by the plates.

3) The heat of the arc and the molten metal joining the workpiece induces heat flow in all three dimensions in the workpiece. Consequently, complex metallurgical changes are caused in the fusion zone or the melt-pool zone due to the severe thermal cycle the metal undergoes. Adjacent to the MPZ, the metal is heated to below the melting point, yet above the eutectoid temperature that causes significant changes in the microstructure and the mechanical properties. This region is known as the heat-affected zone and requires significant attention by design engineers while trying to evaluate the joint strength. The high heat concentration near the center of the arc and the rather sparse heat distribution away from the arc cause nonuniform heating and cooling of the weldment, thus generating plastic deformation and residual stresses in the weldment. This often results in permanent distortions of the weldment.

4) In the heat transfer process, heat is lost from the surfaces in the form of convection and radiation.

5) The drift of the shielding gas causes enhanced convective heat loss from a part of the surface.

In this article, the problem is solved for transient temperature distribution in the plates. The data can be used to determine the heating and cooling rate, weld pool shape and the heat-affected zone. Vaporization is neglected.

Model of Heat Input Energy to the Workpiece

The losses of energy that occur from the arc to the plate are extremely complex in nature and to avoid this complexity a rather obscure term called arc efficiency (η) is used to quantify the energy made available by the arc. $Q = \eta \cdot V \cdot I$ is the energy supplied by the arc. A value of 66 to 69% for η has been reported for GMAW of mild steel by Christensen, *et al.* (Ref. 15), and a value of 71% (±3%) was calorimetrically determined by Essers, *et al.* (Ref. 16), with a wire diameter of 1.2 mm (0.05 in.) and an argon plus 7% CO_2 shielding gas. It may be noted that any change in the welding parameters, such as the shielding gas and its flow rate, electrode shape, nozzle-to-plate distance, welding voltage and current, etc., can significantly affect the arc efficiency value. The data that were used in the present analysis are given in Appendix A and $\eta = 67\%$ was assumed based on the previous work (Refs. 15, 16). The temperature-dependent thermal properties such as conductivity (k) and specific heat (C_p) are available in Refs. 11 and 13. Waszink, *et al.* (Ref. 24), quote Villeminot (Ref. 25) as determining the temperature of the filler metal droplet from melting point to 1000 K above the melting point. For the analysis in this article, a value of 2300 K (melting point plus 550 K) was used as the droplet temperature. The data were provided by the U.S. Army research laboratory. Knowing the welding wire feed rate and the temperature (2300 K) at which the molten droplet separates, we can determine the heat extracted from the arc by the welding wire with the help of the ($C_p - T$) diagram of Ref. 13. It is based on the area under the ($C_p - T$) diagram between the room temperature (298 K) and the droplet temperature (2300 K). Now, $Q = \eta VI$ minus the heat required to melt the welding wire (up to 2300 K) was assumed to be received by the workpiece surface in a radially symmetric Gaussian profile. The Gaussian profile for the arc heat input has almost invariably been used in literature (Refs. 10, 11, 13, 17). Smartt, *et al.* (Ref. 18), also found their experimental data of heat flux to fit the Gaussian profile. Goldak, *et al.* (Ref. 19), used a double ellipsoidal form of the heat input based on the profile.

$$q''(r) = q''_o \exp[-3\, r^2/r_b^2]$$

$$\text{or, } q''(x,y,t) = q''_o \exp\{-3[(x-vt)^2 + y^2]/r_b^2\}$$

where $q''(r)$ = heat flux per unit area per unit time deposited at location r on the plate, q''_o = maximum q'' (at $r = 0$), r = distance from the center of the arc, r_b = arc beam radius describing a region in which 95% of the total heat is deposited on the plate.

A user subroutine DFLUX was written to calculate the heat input distribution in the manner mentioned above, and it was compiled along with the finite element package ABAQUS (Ref. 27) to obtain the temperature distribution in the weldment. Use of ABAQUS for heat flow and stress analysis in a weld was also made by Newman (Ref. 28).

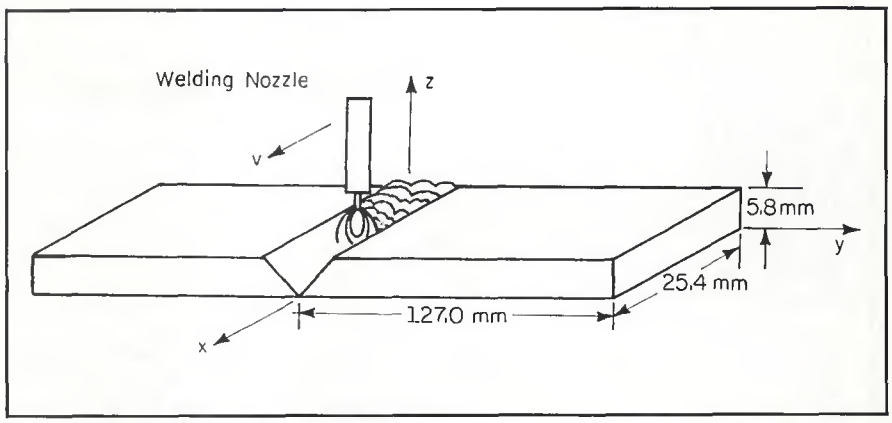

Fig. 1—Illustration of GMA welding process

Energy Equation

The appropriate energy equation without any internal heat generation is:

$$\rho C_p \frac{\partial T}{\partial t} = \underline{\nabla} (k\, \underline{\nabla}\, T) \quad (1)$$

Boundary conditions are given by the Fourier equation:

$$\underline{q}'' = -k\, \underline{\nabla}\, T \quad (2)$$

Heat flux q'' consists of one or more of the following modes of heat transfer depending upon the boundary:

1) $h\ (T - T_a)$, the convective heat loss.

2) $\bar{\epsilon}\sigma\ (T^4 - T_a^4)$, the radiative heat loss.

3) $-q''_s$, if the the surface is receiving a specified heat flux, q''_s.

$q'' = 0$ on $y = 0$ – plane due to symmetry. All other surfaces incur the heat losses due to convection and radiation, and only the top surface (z = thickness) facing the welding gun receives heat flux from the arc.

Theory of the finite element formulation can be found in Ref. 20 and the specifics are discussed in Ref. 13.

Surface Heat Losses

Natural convective heat transfer occurs on all surfaces of the plates except the plane of symmetry ($y = 0$). But the area directly beneath the nozzle of the torch experiences forced convection due to the flow of the shielding gas. Based on previous models (Ref. 9), $h = 10\ W/m^2\ K$ was used for all the surfaces not influenced by the shielding gas, and the following empirical relation initially suggested by Gardon and Cobonpue for air (Ref. 21) and later modified by Steen for any gas (Ref. 22) was used for a part of the top surface under the nozzle of the welding gun:

$$h = 13\ Re^{1/2}\ Pr^{1/3}\ k_{gas}/NPD$$

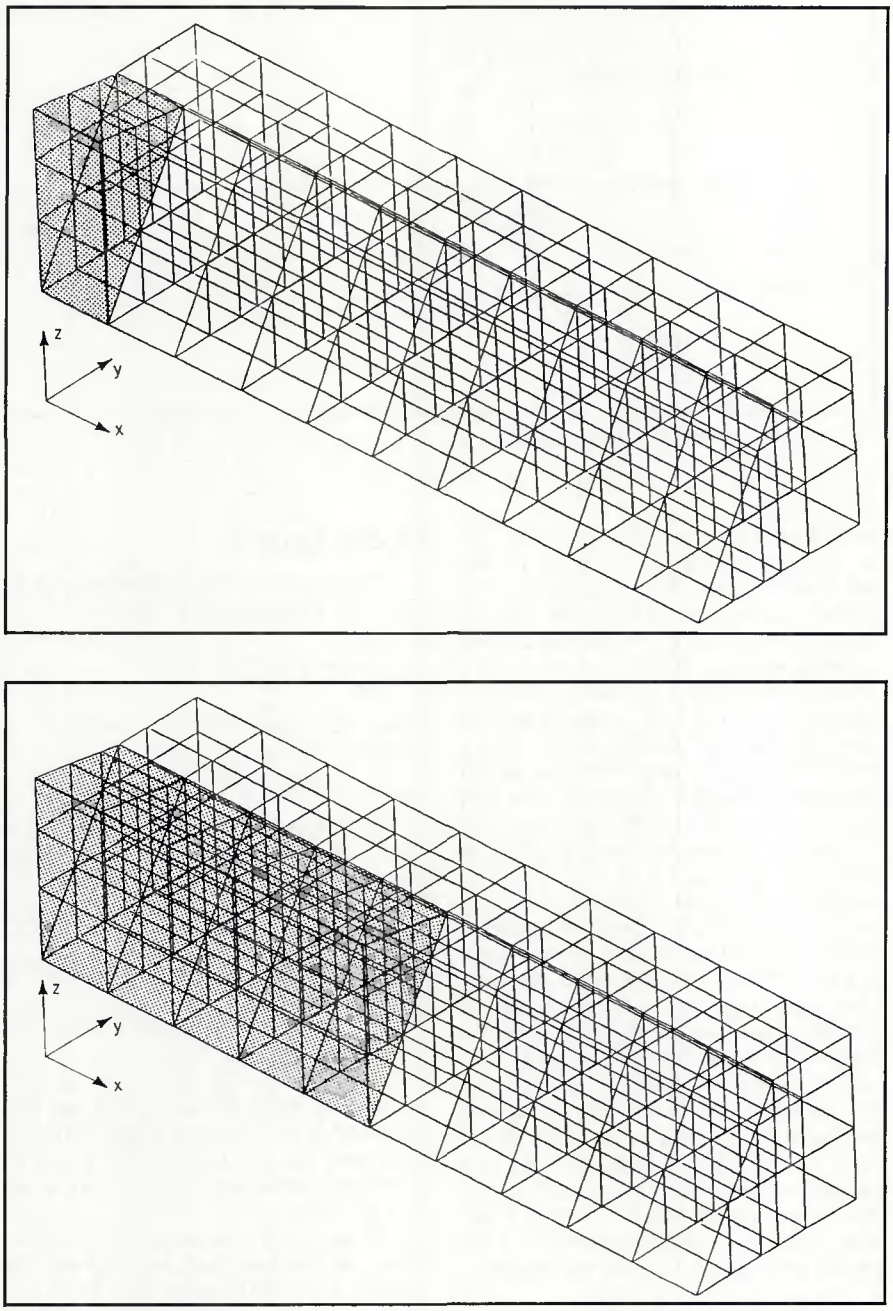

Fig. 2—A—Part of the mesh near V-groove for the first step of FEM analysis. (Filler metal elements are shaded.); B—part of the mesh near V-groove for the fifth step of FEM analysis. (Filler metal elements are shaded)

$$\text{Reynolds number, } Re = \frac{V_{gas} \times D \times \rho_{gas}}{\mu_{gas}}$$

$$\text{Prandtl number, } Pr = \frac{\nu_{gas}}{\alpha_{gas}} = \frac{\mu_{gas}\, C_{P_{gas}}}{k_{gas}}$$

Program HCALC calculates Re and Pr based on the properties of the shielding gas. It then generates subroutine FILM which contains the expression for h. Subroutine FILM is compiled with the main program and calculates h for every integration point at a time step. It may be noted that constant values of h are used for every point under the nozzle. There is no radial variation of h. The heat loss due to convection accounts for a very minor part (less than 5%) of the total heat involved in the process, and hence, a more accurate representation of h will not produce any difference in overall results (Ref. 23).

Radiation heat losses are accounted for all the surfaces except the plane of symmetry ($y = 0$) by using the equation $q'' = \bar{\epsilon}\sigma(T^4 - T_a^4)$. The emissivity value 0.08 has been used.

Mesh Generation

The whole problem is symmetrical about the xz-plane, and hence, it is sufficient to discretize and analyze the plate and the filler metal geometry, which is in the positive octant of the coordinate system shown in Fig. 1.

Choice of a suitable mesh is vital to the accuracy and economy of the finite element results. It may be noted here that the problem of GMA welding is one in which the mesh (or the solution domain, speaking mathematically) grows continuously with time due to the addition of filler metal until welding is completed. Ideally, in order to obtain accurate results, the analysis should be carried out for an infinitesimal length of time, and then the new element or elements (which will be infinitesimally small in size) corresponding to filler metal should be added to the mesh before carrying out the analysis for another infinitesimally small period of time. This alternate process of analysis and redefining the mesh, along with new boundary conditions, will continue until the weld length is covered. However, from a practical point, this is impossible, and we have to opt for an approximate solution by adopting the same scheme of alternating between the analysis and the redefinition of the mesh on the level of finite time and finite size of the filler metal. For the present analysis, the weld length (1 in.) was divided into ten parts and a ten-step analysis was carried out to complete one pass, each step adding a 0.1-in. weld length. Figure 2A shows the mesh for the first step of analysis in which 0.5-s welding time is completed. Then another set of elements is added, and the new boundary conditions are defined before the second step of analysis from 0.5 to 1.0 s is carried out. Figure 2B shows the mesh for the fifth step of the analysis. It may be pointed out that the volume of the additional elements at each step and their size in the welding direction (x-direction) are in agreement with the filler wire feed rate and the welding speed, respectively.

The second important requirement for the mesh is the fine-size elements near the weld centerline. In order to pick the accurate peak temperatures in the heat input area, we must have a certain minimum number of nodes under the arc beam radius. This number depends upon the magnitude of the heat input. The higher the heat input, the more severe is the temperature gradient in the region, and hence, more and more nodes (or degrees of freedom) are required in the region. The authors' experience recommends that at least 5 to 6 nodes should be taken under the arc beam radius for steel materials in order to track the peak temperatures accurately. The temperature distribution is not very sensitive to

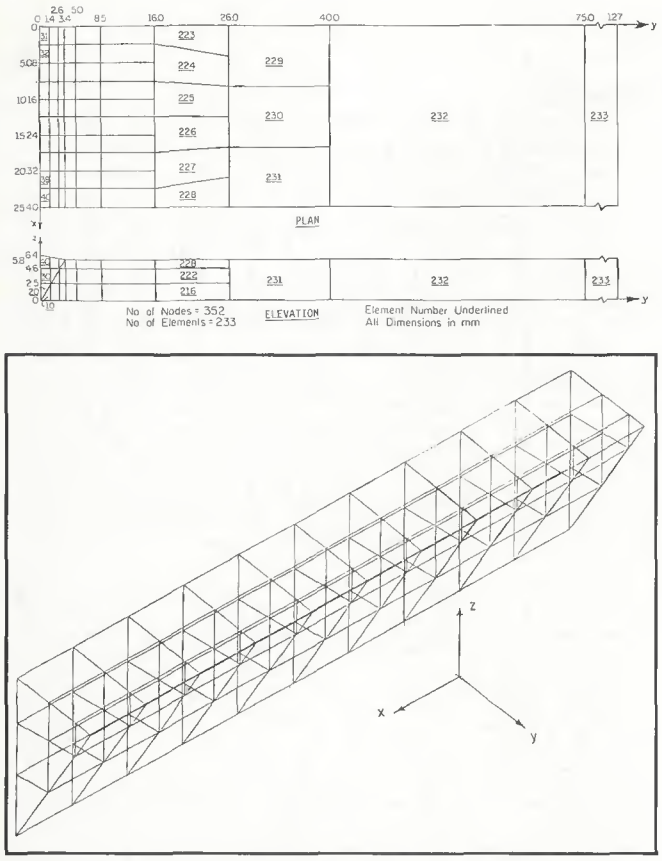

Fig. 3 — A — Orthographic projection of the mesh; B — isometric view of the finite elements of filler metal

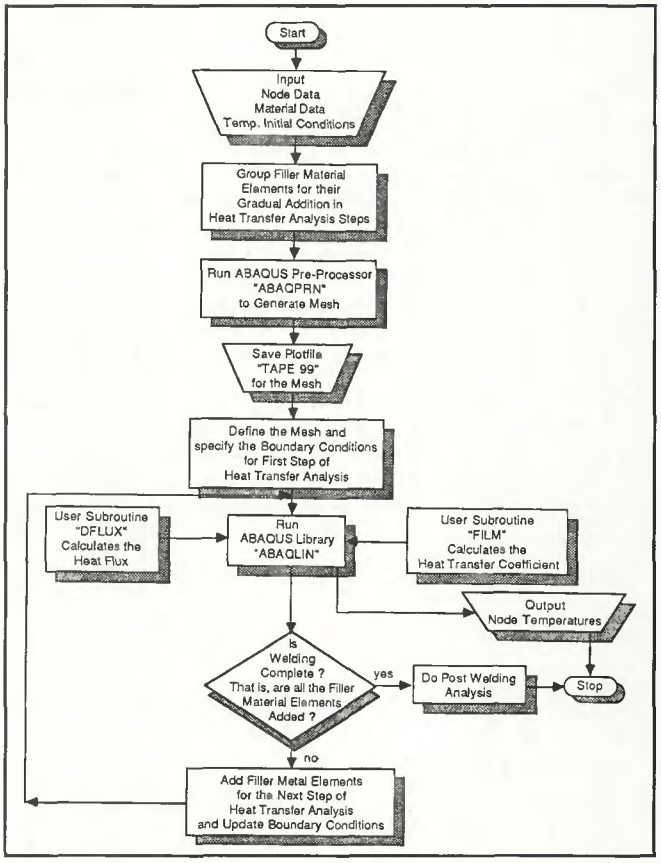

Fig. 4 — Flow chart for the computation scheme

element size far away from the weld centerline, and in order to reduce the cost of analysis, the size of the elements is increased as they get farther away from the region of high heat input. Pammer (Ref. 26) has determined the criterion for the size of elements near the hot boundary to achieve accuracy in the analysis.

Since irregular shape of the boundary poses no threat to the finite element analysis, the boundary of the weld bead can more realistically be modeled. Based on experimental measurements, a 10-deg bulge (Fig. 3) was allowed in the geometry of the filler metal. Since first-order, 8-noded rectilinear elements are more suited for the problems involving latent heat effects (Ref. 27), the same were chosen to discretize the mesh. Some of the elements near the V-groove edge are triangular in cross-section — Fig. 3. ABAQUS uses a $2 \times 2 \times 2$ rule for numerical integration with integration points located at the corners of the element.

The computation scheme using ABAQUS is shown in Fig. 4.

Computed Results and Comparison with Experimental HAZ and MPZ

Figure 5 shows the isotherms on the surface and on the lateral (xz) plane. The curves give the pattern of heat flow in the weldment. These curves are drawn for $V = 28$ V, $I = 380$ A, $\eta = 0.67$ and welding speed = 12 ipm (5.08 mm/s) as supplied by the research laboratory. From Fig. 5C, we notice that the fusion boundary ($T \simeq 1750$ K) is close to the bottom of the plate. Figure 5D shows the region up to $x = 11.3$ mm (0.45 in.) is completely melted at $t = 2$ s after welding started. Weld length (Fig. 1) is 1 in., and it takes 5 s to weld the 1-in. length. Thus, a melt-through is predicted from the numerical results unless there is some support underneath the plates. This was observed to be true experimentally. A lower energy input is sufficient to weld the pieces together.

Thermal history of the material is very important in determining the microstructural changes the material undergoes and the strength of the weld joint. Any suspected critical region can be analyzed by plotting the thermal history in that region. Krutz and Segerlind's results (Ref. 11) indicates that the cooling of metal adjacent to the weld pool is the critical metallurgical location. The thermal histories of the two sample points were drawn in Fig. 6. One point belongs to the HAZ, while the other to the MPZ. Very high temperatures cannot be measured by simple techniques such as with thermocouples. Yet, in the region away from the molten zone, the temperature can be measured and compared in order to get some idea of the accuracy of the numerical results. A thermocouple was attached at location of node 259 (12.7, 8.5 mm) on the surface of the sample and a peak temperature of 1115 K above room temperature was recorded by the thermocouple. Figure 6 shows that the particular location should attain 1200 K above the room temperature. The difference is not very large considering experimental error involved.

The aim of the experiment was to determine the size of the HAZ and the MPZ. Figures 7A and B plot the HAZ and the MPZ boundary at different times and determine the extent of the two regions. The criterion for the HAZ boundary was 1000 K (mild steel) and for the MPZ boundary, 1755 K. Figure 7A shows the time growth of the 1000 K isotherm on the surface. Growth rate is high, up to 6 s of time (note that welding time is 5 s and after this time, no arc heat is supplied to the plates), and then the growth is at a slower rate. The isotherms at $t = 20$ and 24 s are coincident with each other, and then the HAZ decays due to the dominant atmospheric cooling. Thus, the numerical results predict an extent of 16 mm from Fig. 7A in each plate for the HAZ. Experimental observation was found to be 1.25 in. (31.75 mm) when measured across both plates. The numer-

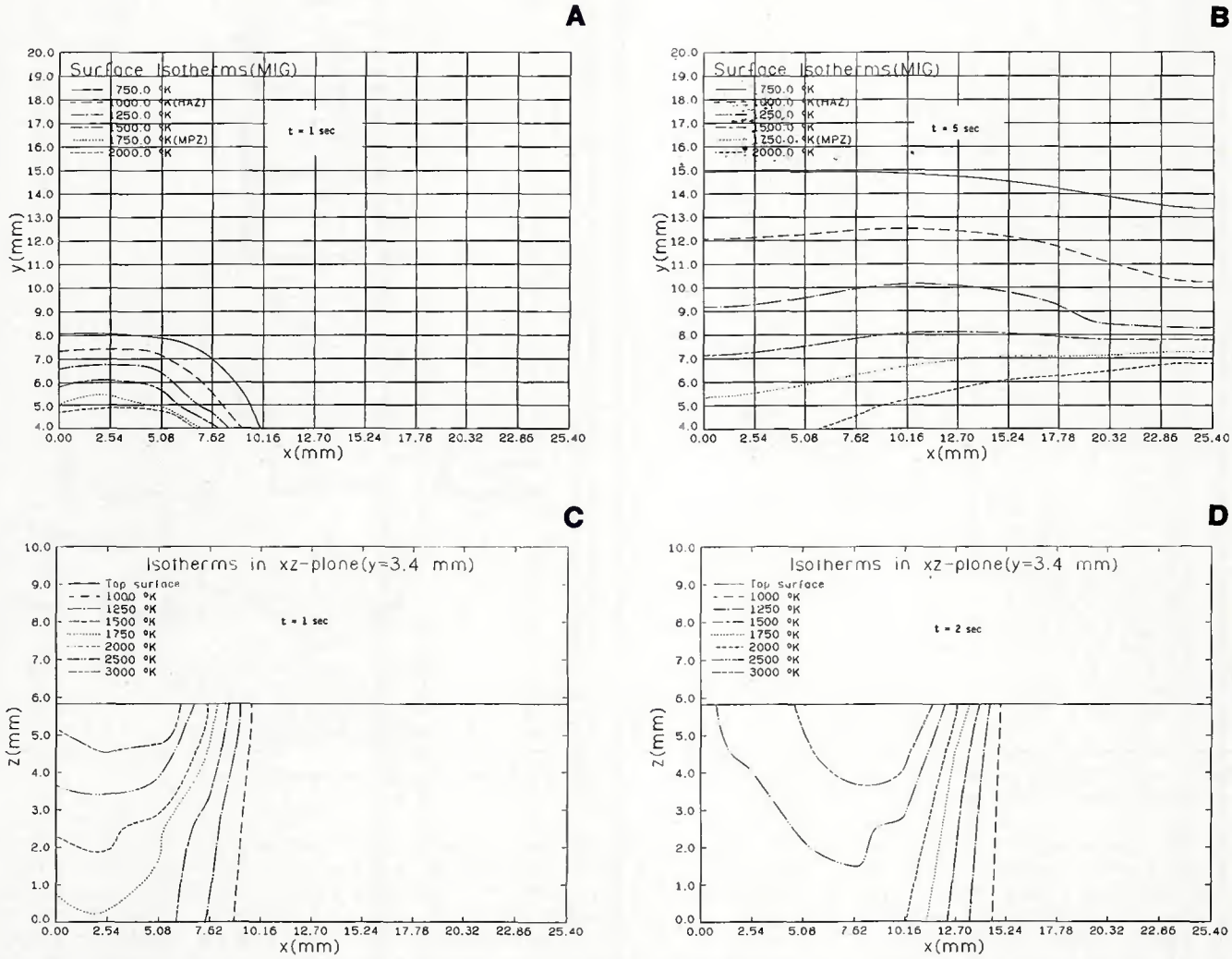

Fig. 5 — A — Isotherms on the top surface; B — isotherms on the top surface; C — isotherms on transverse plane; D — isotherms on transverse plane

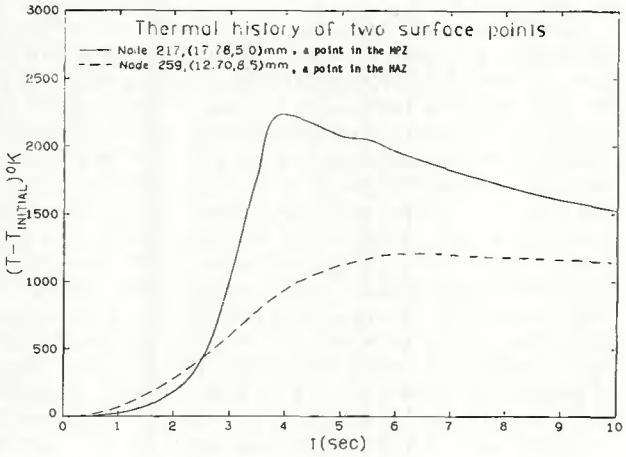

Fig. 6 — Heating/cooling curves of two sample points

ical prediction (16 × 2 = 32 mm) is in very close agreement with the experimental observation. Figure 7B predicts the size of MPZ as 15.4 mm (7.7 mm in each plate) on the surface from finite element calculation. Experimentally, the width of the MPZ was found to be 16.8 mm. These results are shown in Table 1. Figure 7C shows the MPZ between the times 4.5 s and 5 s. The arc is shut off at 5 s when it reaches the edge of the plate. Just before the arc reaches the edge of the plate (at t = 4.9 s and 5 s), a bit sharp rise in the melt-pool width is noticed from Fig. 7C. This rise in the melt-pool width shows up as a kink near t = 4.9 s in Fig. 8 where the sizes of the HAZ and the MPZ have been drawn against time. Size of the HAZ reaches a plateau at t = 20 s. The MPZ width increases for 6 s and then the pool starts solidifying. The reason the melt-pool width increases when the arc approaches the edge is that near the edge of the plate the metal no longer exists further down in the arc travel direction to conduct heat. At the edge

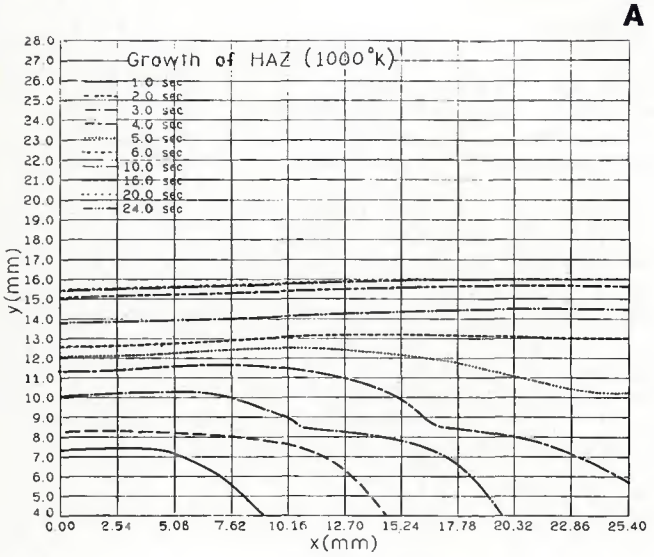

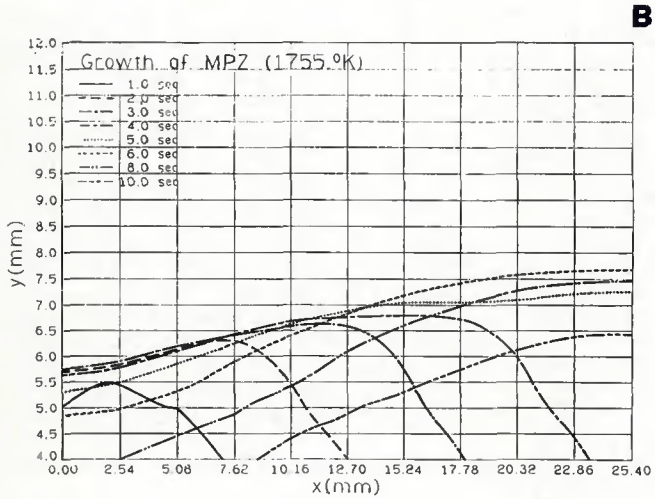

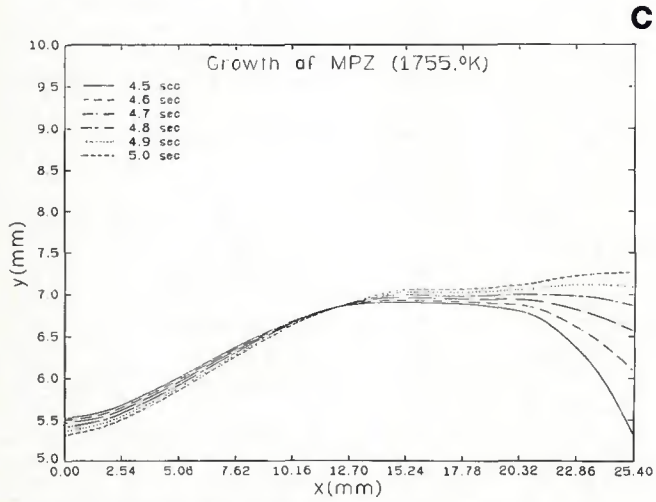

Fig. 7 — A — Numerical determination of the heat-affected zone; B — numerical determination of the melt-pool zone; C — numerical determination of the melt-pool zone

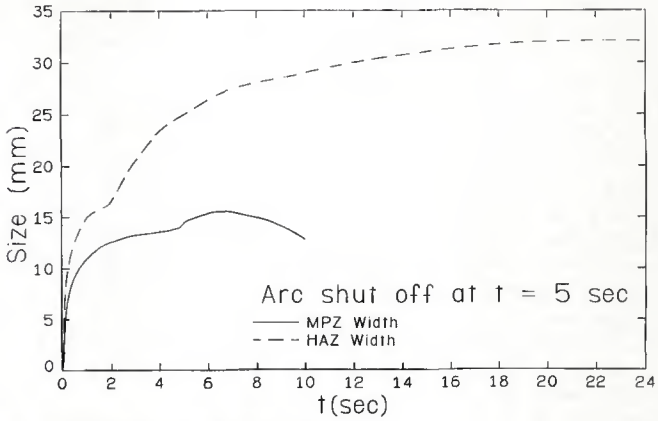

Fig. 8 — Growth of HAZ and MPZ

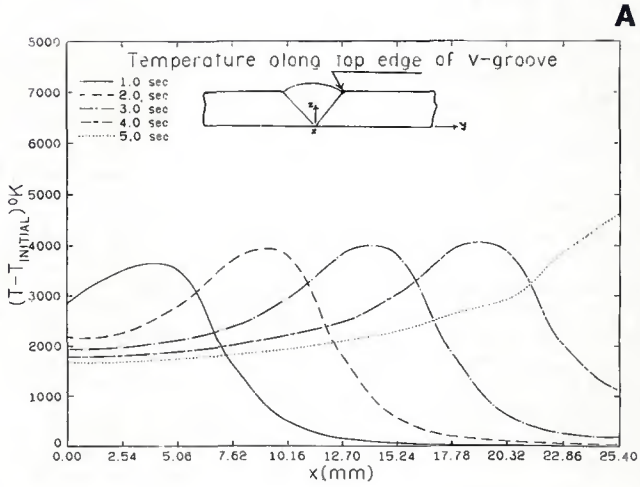

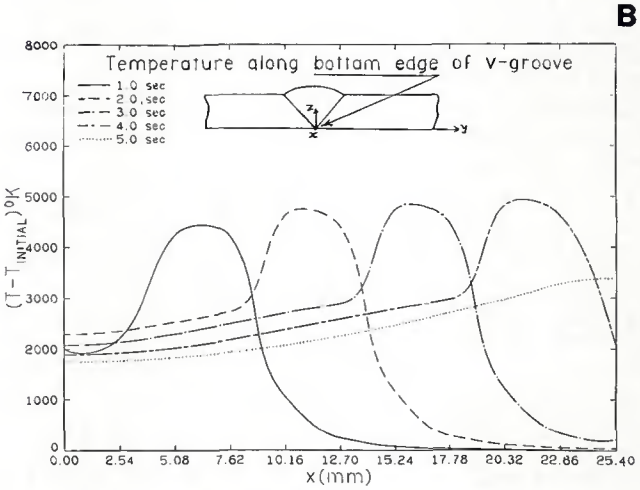

Fig. 9 — A — Transient temperature profile; B — transient temperature profile

are the convective and radiative heat losses which are smaller in amount.

Figures 9A and B plot the temperature distribution along the top and bottom edge of the V-groove at different times after the start of the welding. We may notice in Fig. 9A that the welding speed is faster than the diffusion rate of heat in the material. The peak temperature distribution is not moving at the rate at which the arc is moving. For instance, at t = 1 s, the arc is located at x = 5.08 mm, but the highest temperature is located at about x = 4 mm on the top edge of the V-groove. Similarly, at t = 3 s, the highest temperature is attained by the point x ≃ 14 mm when the arc is passing through the x = 15.24 mm point. In Fig. 9B, we notice the peak temperature distribution moves at almost the same speed as the welding arc. These plots in Fig. 9 also give the estimate of the rate at which points along the V-groove edge cool down.

Conclusions

The following conclusions may be drawn from this analysis.

1) The heat-affected zone increases even after the arc is shut off, indicating the transient analysis is necessary for this process. Quasisteady-state assumption will not be valid for the GMAW process under the given conditions.

2) The metal transfer in GMAW can be simulated by using finite element analysis by adding elements at each time step corresponding to filler metal addition.

3) This paper describes the step-by-step procedure by alternating between the heat transfer analysis and changing the mesh geometry.

4) The predicted HAZ, MPZ and peak temperature as calculated from the analysis were found to be in close agreement with the experimental data.

Acknowledgment

This work was made possible by a contract from the U.S. Army Construction Engineering Research Laboratory, Champaign, Ill. Mr. R. Weber is the program monitor. Mr. Weber's continuous encouragement and invaluable help in the experimental part of the program are highly appreciated.

References

1. Masubuchi, K. 1979. *Welding in The World* 17:11–24.
2. Rosenthal, D. 1941. *Welding Journal* 20(5):220-s to 234-s.
3. Rosenthal, D. 1946. *Trans. ASME* 68:849–866.
4. Boulton, N. S., and Lance Martin, H. E. 1936. *Proc. Inst. Mech. Engrs.* 123:295–347, London, England.
5. Segerlind, L. J. 1976. *Applied Finite Element Analysis.* John Wiley and Sons, Inc.
6. Zienkiewicz, O. C., and Parekh, C. J. 1970. *Int. J. Num. Meth. Engr.* 2:61–71.
7. Wilson, E. L., and Nickell, R. E. 1966. *Nuclear Engr. and Design* 4:276–286.
8. Friedman, E. 1975. J. Pressure vessel technology. *Trans. ASME* (8):206–213.
9. Friedman, E., and Glickstein, S. S. *Welding Journal* 55(12):408-s to 420-s.
10. Friedman, E. January 1980. *DOE Research and Development Report.* Bettis Atomic Power Laboratory, West Mifflin, Pa.
11. Krutz, G. W., and Segerlind, L. J. 1978. *Welding Journal* 57(7):211-s to 216-s.
12. Hibbitt, H. D., and Marcal, P. V. 1973. *Computers and Structures* 3(9):1145–1174.
13. Tekriwal, P., Stitt, M., and Mazumder, J. 1987. *Metal Construction* 19(10):599R–606R.
14. Mahin, K. W., Shapiro, A., and Hallquist, J. May 1986. *Int. Conf. on Trends in Welding Research.* Gatlinburg, Tenn.
15. Christensen, N., Davies, V. de L., and Gjermundsen, K. 1965. *Br. Weld. J.* (2):54–75.
16. Essers, W. G., and Walter, R. 1981. *Welding Journal* 60(2):37-s to 42-s.
17. Pavelic, V., Tanbakuchi, R., Uyehara, O. A., and Myers, P. S. 1969. *Welding Journal* 48(7):295-s to 305-s.
18. Smartt, H. B., Stewart, J. A., and Einerson, C. J. 1985. AWS 66th Annual Convention, Las Vegas, Nev.
19. Goldak, J., Chakravarti, A., and Bibby, M. 1984. *Met. Trans.* 15B(6):299–305.
20. Zienkiewicz, O. C., 1977. *The Finite Element Method.* Third Edition, McGraw Hill.
21. Gardon, R., and Cobonpue, J. 1961. *Int. Heat Transfer Conf.—Part II,* pp. 454–460.
22. Steen, W. M. 1976. Ph.D. Thesis, Imperial College, London, England.
23. Tekriwal, P., and Mazumder, J. 1988. *Metal Construction* (to be published).
24. Waszink, J. H., and Graat, L. H. J. 1983. *Welding Journal* 62(4):108-s to 116-s.
25. Villeminot, P. 1967. *Soudage et Technique Connexes* 21(9/10):367–380.
26. Pammer, Z. 1980. *IJNME* 15:495–505.
27. Hibbitt, Karlsson, and Sorensen. October 1983. *ABAQUS Theory and User's Manuals.* Hibbitt, Karlsson and Sorensen, Inc., Providence, R.I.
28. Newman, S. Z. April 1986. FEM Model of 3D Transient Temperature and Stress Fields in Welded Plate. Ph.D. Thesis, Carnegie-Mellon University, Pittsburgh, Pa.

Appendix A

Data used for numerical results:

Ambient temperature	=	298 K
Filler metal temperature when it joins the V-groove	=	2300 K
Solidus temperature	=	1700 K
Liquidus temperature	=	1755 K
Latent heat of fusion	=	273790 J/kg
Density of mild steel	=	7870 kg/m^3
Welding voltage	=	28 V
Welding current	=	380 A
Arc efficiency, η	=	0.67
Welding speed	=	5.08 mm/s (12 ipm)
Arc beam radius, r_b	=	5.56 mm
Filler wire diameter	=	1.6 mm (1/16 in.)
Filler wire feed rate	=	55.5 mm/s (131 ipm)
Nozzle-to-plate distance	=	19.05 mm (3/4 in.)
Nozzle diameter	=	19.05 mm (3/4 in.)
Nozzle angle with the vertical	=	0 deg

Shielding gas (98% Ar + 2% O_2) data:

Flow rate	=	0.3933 L/s (50 ft^3/h)
Thermal conductivity	=	0.0178 W/m K
Specific heat	=	518.816 J/kg K
Dynamic viscosity	=	2.217×10^{-5} kg/m-s
Density	=	1.7837 kg/m^3

Appendix B

List of Symbols

Cp	Specific heat of metal, J/kg K
Cp_{gas}	Specific heat of shielding gas, J/kg K
D	Nozzle diameter, m
h	Heat transfer coefficient, W/m^2 K
I	Welding current, amperes
k	Thermal conductivity of metal, W/m K
k_{gas}	Thermal conductivity of shielding gas, W/m K
NPD	Nozzle-to-plate distance, m
Pr	Prandtl number of shielding gas
q''	Surface heat flux, W/m^2
q''_s	Specified heat flux on the surface, W/m^2
Re	Reynolds number of shielding gas flow
t	Welding time, s
T	Temperature of metal, K
T_a	Ambient temperature, K
V	Welding voltage, volts
v	Welding speed, m/s
v_{gas}	Shielding gas flow velocity, m/s
x,y,z	Physical coordinates, m

Greek Symbols

α_{gas}	Thermal diffusivity of shielding gas, m^2/s
$\partial/\partial t$	Partial derivative w.r.t. t, 1/s
$\underline{\nabla}$	$\underline{i}\,\partial/\partial x + \underline{j}\,\partial/\partial y + \underline{k}\,\partial/\partial z$, 1/m
$\bar{\epsilon}$	Thermal emissivity
η	Arc efficiency
ν_{gas}	Kinematic viscosity of shielding gas, m^2/s
ρ	Density of metal, kg/m^3
ρ_{gas}	Density of shielding gas, kg/m^3
μ_{gas}	Dynamic viscosity, kg/m-s
σ	Stefan-Boltzman constant $= 5.6697 \times 10^{-8}$ W/m^2 K^4